The Journal of Immunology

EBV Oncogene N-LMP1 Induces CD4 T Cell –Mediated Angiogenic Blockade in the Murine Tumor Model

Tzong-Shoon Wu, Lian-Chen Wang, Shu-Chen Liu, Ting-Yu Hsu, Chun-Yen Lin, Gou-Jin Feng, Jian-Ming Chen, Hao-Ping Liu, I-Che Chung, Tzu-Chen Yen, Yu-Sun Chang, Shuen-Kuei Liao, Chen Chang and Kai-Ping N. Chow

J Immunol 2015; 194:4577-4587; Prepublished online 6 April 2015;
doi: 10.4049/jimmunol.1400794
http://www.jimmunol.org/content/194/9/4577

The Journal of Immunology is published twice each month by
The American Association of Immunologists, Inc.,
9650 Rockville Pike, Bethesda, MD 20814-3994.

Print ISSN: 0022-1767 Online ISSN: 1550-6606.

EBV Oncogene N-LMP1 Induces CD4 T Cell–Mediated Angiogenic Blockade in the Murine Tumor Model

Tzong-Shoon Wu,*[,1,2] Lian-Chen Wang,[†,‡,1] Shu-Chen Liu,[§,¶,1] Ting-Yu Hsu,[†] Chun-Yen Lin,[‖] Gou-Jin Feng,[†] Jian-Ming Chen,[†] Hao-Ping Liu,[#] I-Che Chung,[§] Tzu-Chen Yen, Yu-Sun Chang,[†,§] Shuen-Kuei Liao,[††] Chen Chang,[‡‡] and Kai-Ping N. Chow[†,§§]**

Antivascular immunity may provide long-term protection by preventing neovascularization that precedes tumor progression. Although the tumorigenesis promoted by EBV-encoded oncogene latent membrane protein 1 derived from Taiwanese nasopharyngeal carcinoma (N-LMP1) has been demonstrated, the potential of N-LMP1 for inducing immune surveillance remains elusive. In this article, we describe the immunogenicity of N-LMP1 (1510) and its induction of antivascular immunity in a transplantable tumor model in immunocompetent BALB/c mice. The immunogenicity of N-LMP1 was evaluated on the basis of tumor rejection following immunization. The impact of the immunization on the dynamics of tumor angiogenesis was assessed by temporal noninvasive dynamic contrast-enhanced magnetic resonance imaging and was further confirmed by histologic study and vascular count. Through the experiments of in vivo depletion and adoptive transfer, CD4 T cells were identified as effectors that depend on IFN-γ for tumor prevention. The response was further verified by the identification of an MHC H-2 I-E^d–restricted peptide derived from N-LMP1 and by the immunization of mice with N-LMP1 peptide–loaded dendritic cells. These studies provide insight into N-LMP1–specific immunity in vivo, which suggests that CD4 T cells may play an important role in angiogenic surveillance against LMP1–associated cancer via tumor stroma targeting. *The Journal of Immunology*, **2015, 194: 4577–4587.**

The viral oncogene latent membrane protein 1 (LMP1) plays an essential role in the pathogenesis of a number of EBV-associated malignancies, including nasopharyngeal carcinoma (NPC) endemic in southern China and Taiwan (1). LMP1 demonstrates oncogenicity through promotion of cell transformation, survival, and invasion (1–3). Furthermore, it enhances the production of angiogenic factors and the in vivo formation of the neovasculature for rapid tumor cell expansion and metastasis (1). Intriguingly, LMP1 can also modulate immune genes related to inflammation and Ag presentation (4, 5), which may not only facilitate tumor progression (4) but also put the cells at risk for immune exposure and tumor rejection (6). This finding reveals a crucial role for the in vivo immunogenicity of LMP1 in tumor promotion, especially in cancers such as NPC that arise in the immunocompetent host. Indeed, LMP1-specific CD4 and CD8 T cell responses have been described in healthy virus carriers and cancer patients (7–10). However, the potential clinical benefits of anti-LMP1 immunity against LMP1-expressing tumors remain to be elucidated.

Natural LMP1 variants exist in the human population (11, 12), each possessing different degrees of immunogenicity (13, 14). Among them, LMP1 derived from Taiwanese NPC (N-LMP1; 1510-LMP1) is a variant prevalent in Taiwanese NPC patients with a characteristic 10-aa deletion of Asian variants and additional multiple point mutations different from the Chinese CAO strain (11). N-LMP1 has been demonstrated to be highly oncogenic, using cell lines such as BALB/c-3T3 and NPC-TW01 (15, 16). However, the immunogenicity of N-LMP1 and its relationship to in vivo tumorigenesis remain largely unknown. Considering the involvement of LMP1 in tumor angiogenesis, a prerequisite for tumor progression (17), we explored the possibility that the im-

*Exploratory Research Laboratory, Development Center for Biotechnology, New Taipei City 221, Taiwan, Republic of China; [†]Graduate Institute of Biomedical Sciences, College of Medicine, Chang Gung University, Taoyuan 333, Taiwan, Republic of China; [‡]Department of Parasitology, College of Medicine, Chang-Gung University, Taoyuan 333, Taiwan, Republic of China; [§]Molecular Medical Research Center, Chang Gung University, Taoyuan 333, Taiwan, Republic of China; [¶]Institute of Systems Biology and Bioinformatics, National Central University, Taoyuan 320, Taiwan, Republic of China; [‖]Department of Hepatogastroenterology, Chang Gung Memorial Hospital, Taoyuan 333, Taiwan, Republic of China; [#]Department of Veterinary Medicine, National Chung Hsing University, Taichung 402, Taiwan, Republic of China; **Department of Nuclear Medicine, Center for Advanced Molecular Imaging and Translation, Chang Gung Memorial Hospital, Taoyuan 333, Taiwan, Republic of China; [††]Ph.D. Program for Cancer Biology and Drug Discovery, Taipei Medical University, Taipei 110, Taiwan, Republic of China; [‡‡]Institute of Biomedical Sciences, Academia Sinica, Taipei 115, Taiwan, Republic of China; and [§§]Department of Microbiology and Immunology, Chang Gung University, Taoyuan 333, Taiwan, Republic of China

[1]T.-S.W., L.-C.W., and S.-C.L. contributed equally to this work.

[2]Current address: Institute for Drug Evaluation Platform, Development Center for Biotechnology, New Taipei City, Republic of China.

Received for publication March 28, 2014. Accepted for publication February 23, 2015.

This work was supported by Chang-Gung Memorial Hospital Grants CMRPD180343 and CMRPD1C0062, National Science Council of Republic of China Grant NSC99-2314-B-182-038-MY3, Department of Health of Republic of China Grant DOH100-TD-C-111-008, and National Research Program for Genomic Medicine, National Science Council of Republic of China Grant NSC100-2319-B-001-003 to the Functional and Micro-Magnetic Resonance Imaging Center, Institute of Biomedical Sciences, Academia Sinica, Taipei, Taiwan, Republic of China.

Address correspondence and reprint requests to Prof. Kai-Ping N. Chow or Prof. Chen Chang, Department of Microbiology and Immunology, Chang Gung University, 259 Wen-Hwa First Road, Kwei-Shan, Taoyuan 333, Taiwan, Republic of China (K.-P.N.C.) or Institute of Biomedical Sciences, Academia Sinica, 128 Section 2, Academia Road, Nankang, Taipei 115, Taiwan, Republic of China (C.C.). E-mail addresses: kpc@mail.cgu.edu.tw (K.-P.N.C.) or bmcchen@ibms.sinica.edu.tw (C.C.)

Abbreviations used in this article: DC, dendritic cell; DCE-MRI, dynamic contrast–enhanced magnetic resonance imaging; FOV, field of view; LMP1, latent membrane protein 1; NEX, number of repetitions; N-LMP1, LMP1 derived from Taiwanese NPC; NPC, nasopharyngeal carcinoma; slth, slice thickness; TE, echo time; TPA, 12-*O*-tetradecanoylphorbol-13-acetate; TR, repetition time; TSC, tumor single cell.

www.jimmunol.org/cgi/doi/10.4049/jimmunol.1400794

munogenicity of N-LMP1 may play an important role in immune surveillance against tumor neovessel formation.

To achieve our goal, we evaluated the immunogenicity of N-LMP1 by examining its ability to induce tumor rejection in a transplantable mouse tumor model established by N-LMP1–transformed BALB/c-3T3 (3T3/N-LMP1) cells (18). Tumor single cells (TSCs) prepared from N-LMP1 tumor tissue were irradiated and used to immunize mice before tumor challenge. To study the immune impact during tumor angiogenic transition to exponential growth, we used a series of noninvasive dynamic contrast–enhanced magnetic resonance imaging (DCE-MRI) to assess tumor neovascularization (19) and further confirmed the vascular alteration by histologic study and vascular count. The roles of CD4 and CD8 T cells in immune rejection were further analyzed by in vivo depletion and adoptive transfer. The identification of and immunization with an N-LMP1–derived peptide was pursued to verify the induction of antiangiogenic N-LMP1–specific T cell response in vivo.

Materials and Methods

Mice

Male BALB/c, BALB/cAnN nude, and SCID mice were purchased from the National Laboratory Animal Breeding and Research Center (Nangang, Taiwan). IFN-γ–deficient mice (C57BL/6 background) from The Jackson Laboratory (Sacramento, CA) were fully backcrossed to the BALB/c mice background for 12 generations before use. All mice were maintained under specific pathogen–free conditions in the Animal Care Center of Chang-Gung University and were used at the age of 6–10 wk. The experiments were conducted with the approval of the Chang-Gung University Animal Ethics Committee and the Institute of Animal Care and Utilization Committee.

Tumor cell lines

The N-LMP1 (clone 1510)–transformed BALB/c-3T3 (3T3/N-LMP1) stable clones E2 and E9, and 3T3/Neo cells containing the vector alone, were established and maintained as previously described (15, 18). The E2-plus tumor cell line was recovered and established from an E2 tumor (18). The Ras oncogene–transformed BALB/c-3T3 (3T3/Ras) clone LZEJ was a gift from Dr. Wen-Chang Lin (20) (Institute of Biomedical Sciences, Academia Sinica, Taiwan). CT26/N-LMP1 and CT26/Neo cells are CT26 cells (a mouse colon carcinoma cell line) that were transfected with the N-LMP1 gene or vector alone, respectively (21). B95.8 is an EBV-transformed lymphoid cell line that secretes LMP1-containing exosomes (22, 23).

N-LMP1 tumor model

A transplantable N-LMP1 tumor model was established via the oncogenicity of N-LMP1, as previously described (18). Briefly, tumors were initiated in SCID mice by 3T3/N-LMP1 and subsequently transferred into BALB/c mice by fragment transplantation. The tumors were passaged among BALB/c mice every 3–4 wk to maintain the tumor line in vivo. The day of transplantation was referred to as day 0. The tumor volumes were measured with a caliper and calculated using the following formula: volume = $d_1 \times d_2 \times d_3 \times 0.5236$, where d_n represents the three orthogonal diameter measurements. A tumor with a minimal size of 40 mm^3 was scored as positive.

Preparation of TSCs, immunization, and tumor challenge

TSCs were prepared by enzyme digestion of the tumor mass as previously described (18). The 3T3/Ras TSCs were from LZEJ-induced tumors (10^6 per mouse). For immunization, 4000 R–irradiated (Gammacell 3000 Elan, MDS Nordion, Ottawa, ON, Canada) TSCs, 3T3/Neo cells (2×10^6 per mouse), or peptide-loaded dendritic cells (DCs) (1×10^6 per mouse) were injected s.c. into the right flank of the mice. At 4 d later, mice were contralaterally challenged with N-LMP1 (E2) tumor fragment. Alternatively, CT26 tumors were induced by s.c. injection of CT26/N-LMP1 or CT26/Neo cells (2×10^5 per mouse), respectively.

Magnetic resonance imaging

MRI experiments were performed on a horizontal 7.0 T Pharma Scan 70/16. Experimental procedures and imaging data acquisitions were carried out according to our previous study (19). In brief, imaging was performed on days 3, 7, 9, 11, and 14 after tumor transplantation. A 38-mm birdcage coil was used for radiofrequency excitation and signal reception, and no triggering was used for data acquisition. To generate T2 maps and determine tumor volume, multislice multiecho axial images were acquired using standard spin-echo sequences with a repetition time (TR) of 5000 ms; echo times (TEs) of 10.4, 20.8, 31.2, 41.6, 52, and 62.4; a field of view (FOV) of 3 cm; a number of repetitions (NEX) of 2; a matrix size of 256 × 128 (zero filled to 256 × 256); and a slice thickness (slth) of 0.5 mm, with no interslice gaps. Precontrast T1 maps were acquired by inversion-recovery-fast imaging with a steady-state precession sequence having a TR of 4 ms, a TE of 1.8 ms, a FOV of 3 cm, a slth of 1.5 mm, a NEX of 1, a flip angle of 60°, a matrix size of 128 × 128, and 18 inversion times, ranging from 62 to 2510 ms with an increased interval of 144 ms. DCE-MRI was performed using a T1-weighted spin-echo sequence with a TR of 400 ms, a TE of 10.4 ms, a FOV of 3 cm, a slth of 1.5 mm, a NEX of 1, and matrix size of 256 × 64 (zero filled to 256 × 256). A series of 40 axial images were acquired before, during, and after i.v. injection of the contrast agent gadopentic acid (Magnevist; Schering, Berlin, Germany) at a dose of 0.2 mmol/kg.

For quantification of tumor volume, the region of interest was manually outlined from each of the multislice axial T2-weighted images, and the sum of all regions of interest was calculated as the total tumor volume. Measurement of the volume transfer constant, K^{trans}, between the plasma and the extravascular extracellular space, was performed by the kinetic analysis of dynamic gadopentic acid signal enhancement based on the compartment model of Tofts and Kermode (24). In this analysis, the rate of contrast agent uptake, dCt(t)/dt, can be determined by the product of the permeability (P) and surface area (S), the tracer concentration in arterial blood plasma (Cp), the tracer concentration in tissue (Ct), and the leakage space per unit volume of tissue (ve), according to the following equation:

$$\frac{dC_t(t)}{dt} = K^{trans}Cp(t) - \left(\frac{K^{trans}}{ve}\right)C_t(t),$$

where K^{trans} is equal to PS. The dynamic signal-enhanced curve was fitted on a pixel-by-pixel basis using nonlinear regression analysis to yield a parametric map of K^{trans}.

Tumor histology and quantitation of neovessels

Tumor paraffin sections (5 μm) were stained with H&E, using the standard procedures. To quantify the tumor neovessels, mice were anesthetized by the i.p. injection of tribromoethanol [(Avertin), 660 mg/kg; Sigma-Aldrich, St. Louis, MO] and perfused transcardially with PBS buffer for 2 min, followed by 10% India ink/gelatin solution for 20 s. The solution was freshly prepared by mixing India ink solution (Creative Microbiologicals, Taipei, Taiwan) with 50–60°C preheated 2% gelatin (25). The rate of perfusion was 6 ml/15 s. Afterward, the mice were placed on ice for 30–60 min to allow solidification of the gelatin before tumor removal for cryostat sectioning at 10 μm. Whole tissue sections were imaged by HistoFAXS (TissueGnostics, Vienna, Austria) using a Zeiss microscope at a ×200 final magnification. The images were further processed to improve the black-and-white contrast, and the black areas were quantified using ImageJ software. The average of the three largest tumor areas per tumor was given.

In vivo depletion and enrichment of CD4 and CD8 T cells

For in vivo depletion of CD4 or CD8 T cells, the mice were i.p. injected with the mAbs GK1.5 (rat IgG_{2b}) or 2.43 (rat IgG_{2b}) over 3 successive days (25 μl ascites per mouse per day). Vaccination was conducted 1 d later. For adoptive transfer or in vitro T cell activation, splenic CD4 or CD8 T cells were positively selected using magnetic separation (Miltenyi Biotec, Bergisch Gladbach, Germany) according to the manufacturer's instructions. The in vivo depletion of CD4 or CD8 T cells and the purity of T cell subpreparations were confirmed using flow cytometric analysis, which showed >90% specific depletion and >90% purity of the enrichments.

Flow cytometric analysis

Cells were washed with cold FACS buffer (1% FCS-PBS) and stained with fluorescein-labeled mAb according to the manufacturer's protocol. The cells (10^4 per sample) were analyzed on a FACScan cytometer using CellQuest software. In all cases, cells were gated according to size and scatter to eliminate debris.

Preparation of N-LMP1–presenting DCs and MHC-II$^+$ stromal cells

DCs were prepared as previously described, with modification (26). In brief, normal spleens were fragmented and enzyme digested, followed by

NycoPrep 1.077 fractionation. CD11c$^+$ cells in the low-density fraction were positively selected using an autoMACS Separator (Miltenyi Biotec). In some experiments, the low-density cells were sorted for CD45$^+$CD11c^{hi} population, using the FACSAria system [Becton Dickinson (BD), Los Angeles, CA]. The purity of CD11c$^+$ DCs was routinely >95%. For N-LMP1 Ag presentation, purified DCs (2×10^5) were cultured with frozen/thawed E2-plus cells (8×10^4) or with the indicated N-LMP1 peptide (0.01 M; Kelowna International Scientific, Taipei, Taiwan) in a total volume of 200 μl RPMI containing 10% FBS and GM-CSF (10 ng/ml; Sigma-Aldrich) in 96-well plates for 1 h. Afterward, DCs were further activated for 30 min by LPS (1 μg/ml; Sigma-Aldrich) and polyinosinic-polycytidylic acid (20 μg/ml; Sigma-Aldrich) before in vitro or in vivo use. Tumor-associated MHC-II$^+$ stromal cells were identified by staining TSCs with anti-CD11b–PE (M1/70, BD) or anti-I-A^d/I-E^d–biotin (2G9) and PE-Cy7–conjugated streptavidin (eBioscience). The purity of MHCI-II$^+$ cells after sorting was routinely >90%.

CD4 T cell stimulation and IFN-γ assay

DCs were mixed with primed CD4 T cells at a 1:4 DC/T cell ratio in a total volume of 200 μl. Supernatants were collected at 72 h for the measurement of IFN-γ, using the DuoSet ELISA kit (R&D Systems, Minneapolis, MN). An anti-IE^d mAb was purchased from Abcam (Cambridge, U.K.).

Immunoblot analysis

Cultured cells were lysed in Nonidet P-40 lysis buffer, and equal amounts of protein were separated by NaDodSO$_4$-PAGE and transferred to polyvinylidene fluoride membranes. After blocking with 5% BSA (Sigma-Aldrich), membranes were probed with primary Abs against LMP1 (S12) (1:2000), HSP70 (1:2000) (System Biosciences, Mountain View, CA), CD81 (1:2000) (System Biosciences), or GAPDH (1:3000) (Abcam), followed by incubation with HRP-conjugated secondary Ab and development with ECL detection reagents.

Exosome isolation and transfer

Cells were cultured in complete DMEM at a density of 1×10^6 cells per 10 ml for overnight. The media were replaced with serum-free DMEM for 48 h. The culture supernatants were then collected for total exosome isolation, using the ExoQuick-TC kit (System Biosciences) according to the manufacturer's instructions (27). The isolated exosome pellets were either lysed in 100 μl 1% Nonidet P-40 lysis buffer for immunoblot analysis or resuspended in 100 μl PBS and stored at −80°C until use. B95.8 cells, with or without 12-*O*-tetradecanoylphorbol-13-acetate (TPA) (Sigma-Aldrich) (30 ng/ml) treatment, were used as LMP1 positive controls (22). For exosomal uptake, purified MHC-II$^+$ cells (10^6) were coincubated with 50 μl exosomes at 37°C for time points indicated. Afterward, cells were stringently washed with PBS, and total proteins were collected for the immunoblot analysis.

Angiogenesis assay

In vivo angiogenesis assays were conducted by injecting 0.3 ml growth factor–reduced Matrigel containing 2×10^5 MHC-II$^+$ stromal cells. At 8 d after implantation, the blood flow in the Matrigel implants was visualized and measured by high-resolution ultrasound microimaging using the VEVO 2100 Ultrasound with a 40-MHz transducer in three-dimensional power Doppler mode (VisualSonics, Toronto, ON, Canada). The percentage of the Matrigel implant volume with detectable blood flow was calculated using the three-dimensional segmentation tool in the VEVO 2100 software package (28). Afterward, the Matrigel implants were harvested for histologic examination by H&E staining.

Statistical analysis

Data are presented as the mean values ±SD. Statistics were evaluated using a two-tailed test. A p value < 0.05 was considered statistically significant.

Results

The induction of early tumor angiogenic arrest by immunization

To examine the in vivo immunogenicity of N-LMP1, BALB/c mice were immunized with PBS or irradiated N-LMP1–containing TSCs (N-LMP1) prepared from a tumor that was induced by the 3T3/N-LMP1 stable clone E2. The nontumorigenic 3T3/Neo (Neo) were injected to serve as a 3T3 cell background control. At 4 d later, the mice were challenged with an E2 tumor by the implantation of a tumor fragment on day 0. To assess the kinetics of immune rejection, tumor development was observed by MRI because of its high resolution (19). Fig. 1A demonstrates a detectable gradual increase of tumor volume in days 3–14 of the PBS and Neo groups. However, tumor growth was retarded in the N-LMP1 group. Previously, we identified an angiogenic time window (days 7–14) accompanying this mild tumor expansion, using volume transfer constant (K^{trans}) analysis of DCE-MRI (19). To understand the influence of immunization on the early angiogenesis that precedes N-LMP1 tumor exponential growth after day 14 (18, 19), we evaluated the temporal change of K^{trans} in mice receiving PBS or N-LMP1 in the immunization. The temporal K^{trans} maps and corresponding direct photographs are shown in Fig. 1B. The K^{trans} maps of the PBS group illustrated that leaky vessels developed from the tumor periphery on day 3 and rapidly penetrated the whole tumor within 2 wk. However, high K^{trans} values were absent in the N-LMP1 group. Quantitative analysis of the temporal changes in the spatial dependence of K^{trans} profiles within the tumor is shown in Fig. 1C. The PBS group simultaneously developed multiple peaks with rising K^{trans} values during tumor expansion, indicating that multiple angiogenic active sites are merging together during early neovascularization. However, these angiogenic activities were suppressed by a previous immunization.

The tumor neovasculature in day 7 tumor tissues in the PBS and N-LMP1 groups was next examined histologically. As shown in Fig. 2A, control PBS-treated tumors contained blood vessels with irregular diameters and branches distributed within the tumor tissue that was newly grown from the implanted tumor fragment. Patches of hemorrhage were seen in the tumors of the N-LMP1 group of mice, suggesting vascular damage resulting from immune surveillance. To further quantify the angiogenic activity, blood vessels were labeled in vivo with India ink by perfusion (Fig. 2B). The images of black-filled dots and strips in frozen sections were further processed and quantified using ImageJ software. Fig. 2C illustrates a significantly lower number of blood vessels in the N-LMP1 group tumors than in control tumors, confirming that immunization reduced tumor angiogenesis.

The immunogenicity of N-LMP1

To further determine the immunogenicity of N-LMP1 responsible for successful immunization, mice were immunized with PBS, irradiated 3T3/Neo cells, 3T3/Ras TSCs, and 3T3/N-LMP1 TSCs (from clone E2- or E9-induced tumor) 4 d before E2 tumor challenge on day 0. As indicated in Fig. 3A, tumors developed in all of the control mice, with exponential growth occurring after day 14. Whereas all of the mice receiving 3T3/Neo and 3T3/Ras TSCs also developed tumors, tumor growth was inhibited in E2 or E9 TSC-immunized mice. The result suggested that the immunogenicity of N-LMP1 caused effective tumor rejection in vivo.

Because NPC-derived LMP1 variants were notable for their nonimmunogenicity or low immunogenicity (13, 14), the N-LMP1–induced protective effect along the extending period of time elapsed after immunization was verified next (Fig. 3B). The mice receiving immunization from 4 to 28 d prior to tumor challenge exhibited varying degrees of tumor inhibition. Among these animals, both day (−4) and day (−7) groups had full protection, indicating that N-LMP1 could indeed induce an antitumor response, which was optimal 4–7 d after administration.

The T cell immunity induced by N-LMP1

The in vivo immunogenicity of an Ag relies on both the Ag itself and the immune responsiveness of the host (29). To examine the protective role of T cells, we verified the immune effect in nude mice (Fig. 4A). In contrast to BALB/c mice, nude mice immu-

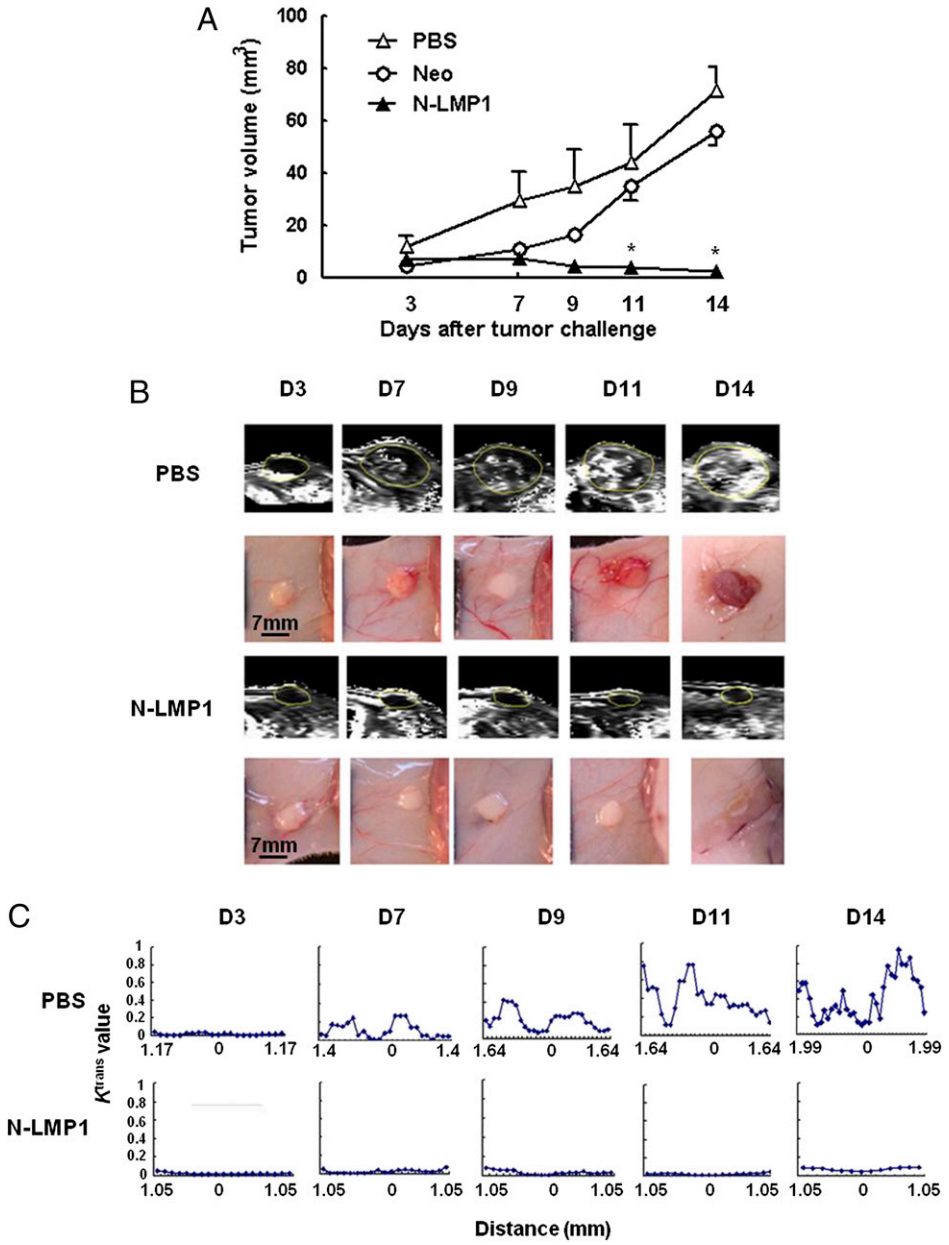

FIGURE 1. Detection of tumor inhibition and angiogenic blockade by MRI. BALB/c mice were immunized with PBS, or with 3T3/Neo (Neo) or N-LMP1 TSCs (N-LMP1), and then challenged with tumors ($n = 4$). (**A**) The tumor growth curve was calculated from MRI analysis. A statistically significant difference between N-LMP1 and PBS or Neo groups was observed on days 11 and 14. $*p < 0.05$. (**B**) DCE-MRI was serially performed on the PBS- or N-LMP1–immunized individuals during days 3–14. Representative K^{trans} maps for each data point are shown. The yellow circles defined the tumor tissue for analysis. The direct photographs of vessel development on each corresponding day were taken from another group of mice that received the same treatment. (**C**) Spatial distribution of K^{trans} profiles from the tumor center to the edge is depicted as a function of distance.

nized with either PBS or N-LMP1 developed tumors, suggesting that T cell competency is required to protect against N-LMP1 tumors. The important T cell subset (CD4 or CD8) in BALB/c mice responsible for tumor rejection was next examined by in vivo depletion using specific Abs prior to the immunization and tumor challenge. Fig. 4B demonstrates full protection in the absence of CD8 T cells. However, the protection was completely abolished when CD4 T cells were depleted (Fig. 4C), indicating an essential role for CD4 T cells in the tumor defense demonstrated.

Owing to the nontumorigenic property of 3T3/Neo, we used a colon cancer CT26 tumor system in BALB/c mice to further validate the induction of CD4 T cell immunity by N-LMP1 independent of the CD8 T cell response. SCID mice underwent adoptive transfer with normal CD4 or CD8 T cells prior to CT26/N-LMP1 tumor challenge. Fig. 5A illustrates that only mice receiving CD4 T cells showed tumor growth inhibition, indicating that they were the effectors. Because IFN-γ is essential in CD4 T cell–mediated antitumor immunity (30–32), CD4 T cells from IFN-γ–deficient mice were also transferred into SCID mice and compared with normal CD4 T cells. The inability of IFN-$\gamma^{-/-}$ CD4 T cells to inhibit tumor progression (Fig. 5A) suggested that the N-LMP1–induced CD4 T cell immunity was also mediated by IFN-γ. To verify that the induction of the CD4 T cell response was specific to N-LMP1, another set of SCID mice was challenged with CT26/Neo tumor cells with or without CD4 T cell transfer (Fig. 5B). CT26/Neo tumor growth was not attenuated by CD4 T cell transfer. These results suggest a direct link between N-LMP1 immunogenicity and CD4 T cell–mediated host immune defense.

Mapping of CD4 T cell response to N-LMP1 peptide

To further validate the induction of CD4 T cell immunity by N-LMP1, we evaluated the N-LMP1 responsiveness of primed CD4 T cells in vitro. CD4 T cells from N-LMP1–immunized mice were restimulated with DCs precultured with or without dead E2-plus cells that provided the N-LMP1 Ag. To facilitate the T cell IFN-γ response, we treated DCs with LPS and polyinosinic-polycytidylic acid after the E2-plus coculture for optimal IL-12 production. The supernatants of the CD4 T–DC coculture were tested for IFN-γ release by ELISA. Fig. 6A shows that primed CD4 T cells produced little IFN-γ. The addition of DCs enhanced IFN-γ production, and

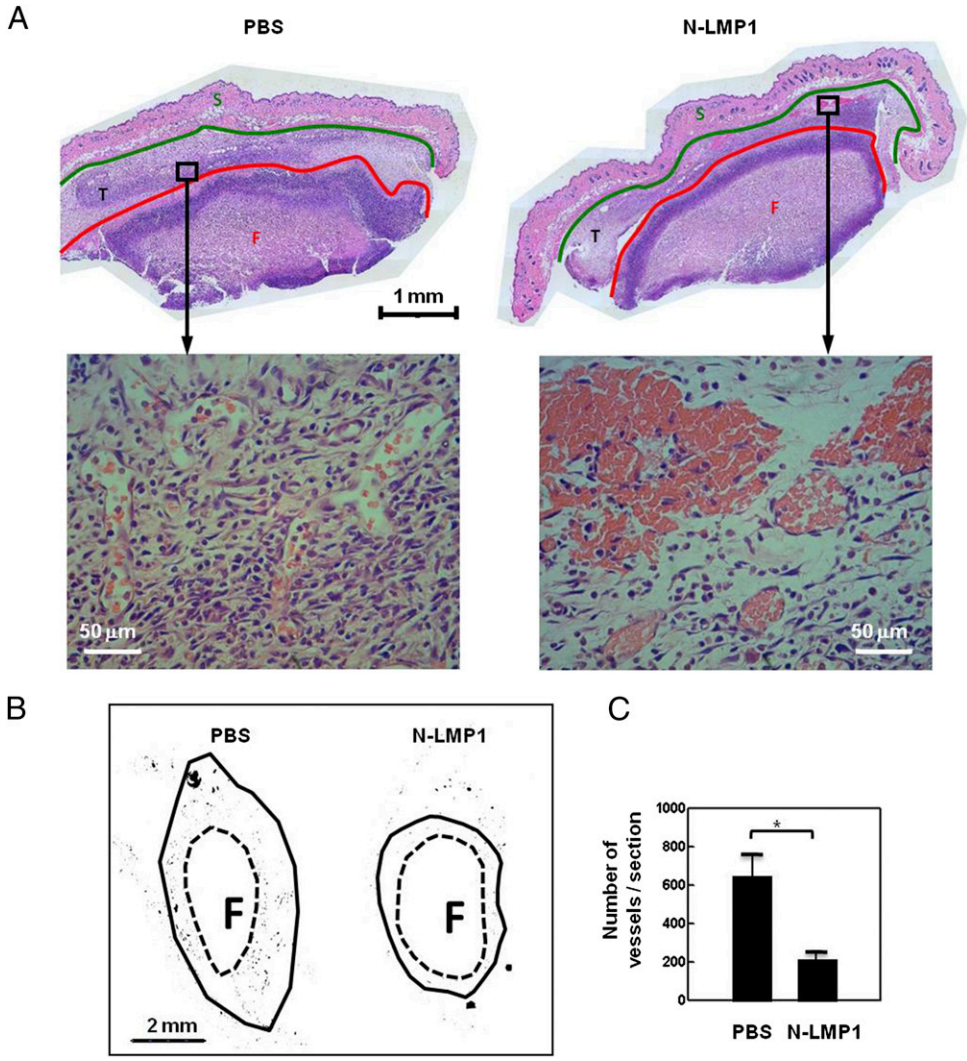

FIGURE 2. Morphologic and quantitative study of the angiogenic blockade. (**A**) Representative H&E-stained day 7 tumor sections from the PBS and N-LMP1 groups ($n = 4$). The two groups of mice ($n = 3$) were perfused with India ink to label the neovessels in vivo. The perfused tissue sections were shown (**B**), and the vessels were further quantified (**C**) as described in *Materials and Methods*. Statistically significant difference between N-LMP1 group and PBS control is indicated. $*p < 0.05$. F, implanted tumor fragment; S, skin layer; T, new tumor tissue.

N-LMP1–preloaded DCs further boosted the response, suggesting that the N-LMP1 activated CD4 T cells in vivo.

To locate the regions of CD4 T cell recognition, eight candidate peptides in the N-LMP1 sequence predicted to bind to mouse MHC-II molecules were synthesized and tested in vitro for their ability to stimulate primed CD4 T cells using peptide-pulsed DCs. Fig. 6B demonstrates that only one peptide ($N\text{-}LMP1_{186–194}$) could elicit IFN-γ augmentation. Next, the matching MHC-II allele for Ag presentation was determined by the addition of an anti–$I\text{-}E^d$ blocking Ab. As shown in Fig. 6C, the production of IFN-γ decreased with increases in the Ab concentration, indicating that $N\text{-}LMP1_{186–194}$ is presented in the context of $I\text{-}E^d$.

The antitumor effect of N-LMP1 peptide–loaded DCs in vivo

As in vitro activated DCs may stimulate CD4 T nonspecifically (Fig. 6A), we verified the antitumor function of $N\text{-}LMP1_{186–194}$ in vivo. Normal mice were immunized with DCs alone or with control peptide $N\text{-}LMP1_{1–10}$– or $N\text{-}LMP1_{186–194}$–loaded DCs 4 d before challenge by tumor fragment transplantation (Fig. 6D). Tumor development was suppressed only in mice immunized with $DC/N\text{-}LMP1_{186–194}$, confirming the ability of N-LMP1 to induce specific CD4 T cell responses.

The potential target of N-LMP1–specific CD4 T cells

CD4 T cells may be stimulated by tumor cells that express MHC-II. As the MHC-II expression may be induced by IFN-γ, we examined MHC-II on tumor cells by flow cytometry, using CT26/N-LMP1 or E2-plus cells that had been cultured with or without IFN-γ for 2 d (Fig. 7A). Neither cell line exhibited MHC-II even with IFN-γ stimulation. Alternatively, T cells may recognize stromal cells that present tumor Ags captured from surrounding cancer cells (33). We have demonstrated that infiltrates bearing CD11b, a marker for the myeloid monocytic lineage of cells, are abundant in N-LMP1 tumor (18). To evaluate the potential recognition of stromal cells by N-LMP1–specific CD4 T cells, TSCs were examined for the expression of MHC-II and CD11b by flow cytometry. MHC-II expression was mainly associated with $CD11b^+$ cells (Fig. 7B). Next, the $MHC\text{-}II^+$ cells were sorted and analyzed for IFN-γ production by CD4 T cells primed by $N\text{-}LMP1_{186–194}$–loaded DCs (Fig. 7C). The IFN-γ production was significantly higher in the coculture than in CD4 T or $MHC\text{-}II^+$ cells alone, suggesting the in vivo presentation of N-LMP1 Ag by tumor-surrounding $MHC\text{-}II^+$ cells.

Tumor cells carrying latent EBV were shown to release exosomes containing LMP1 (34). To further assess the possibility of

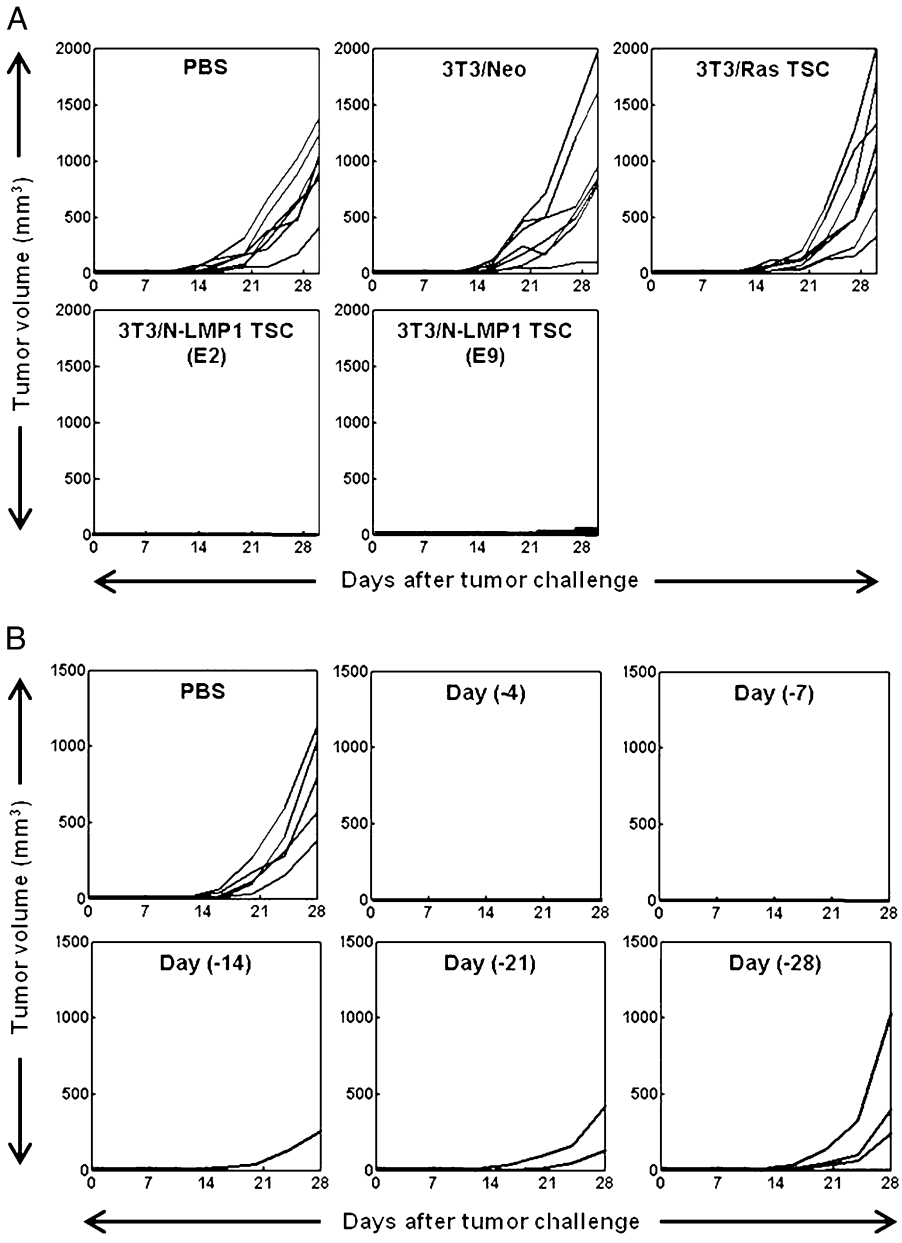

FIGURE 3. Induction of tumor rejection by N-LMP1. BALB/c mice were immunized with (**A**) PBS, 3T3/Neo, 3T3/Ras TSCs, 3T3/N-LMP1 E2, or E9 TSCs ($n = 7$) at −4 d or (**B**) E2 TSCs ($n = 5$) at −4, −7, −14, −21, or −28 d prior to E2 tumor challenge on day 0. Tumor growth curves of individual mice are presented as a function of time after tumor challenge.

intercellular transfer of N-LMP1 from tumor to stromal cells, we examined the LMP1 protein in exosomes purified from the culture supernatants of 3T3/Neo or 3T3/N-LMP1 cells in comparison with the whole-cell lysates, using immunoblot analysis. The relative levels of LMP1 expression were compared with an EBV-positive cell line, B95.8, that secretes LMP1-containing exosomes (22, 23). As shown in Fig. 7D, B95.8 cells treated with TPA for 48 h exhibited increased LMP1 levels in both cell lysates and exosomes, as expected. Although LMP1was undetectable in either preparation derived from 3T3/Neo cells, it was abundant in 3T3/N-LMP1 counterparts. The standard exosomal markers HSP70 and CD81 were detected in all exosome preparations. Thus, 3T3/N-LMP1 resembles EBV-harboring tumor cells, releasing exosomes containing abundant LMP1 protein. Next, the potential for internalization of exosomes by MHC-II$^+$ stromal cells was evaluated by coculturing MHC-II$^+$ cells with 3T3/Neo- or 3T3/N-LMP1–derived exosomes for 1 or 3 h. Following extensive cell washing, cell lysates were prepared and examined for LMP1 protein by immunoblotting. As shown in Fig. 7E, LMP1 was detected only in MHC-II$^+$ cells exposed to purified exosomes secreted from 3T3/N-LMP1, but not from 3T3/Neo, cells. The results suggest that MHC-II$^+$ cells can uptake LMP1-containing exosomes and that LMP1 Ag is likely to be transferred from tumor cells to neighboring MHC-II$^+$ stromal cells through mechanisms such as uptake of exosomes.

To obtain further evidence for the role of CD4 T cells in the control of tumor neovascularization, we conducted an in vivo Matrigel angiogenesis assay stimulated by MHC-II$^+$ stromal cells. The MHC-II$^+$ cells were sorted, mixed with Matrigel, and injected (s.c.) into mice receiving PBS or N-LMP1 immunization 4 d before. The vascularization in the Matrigel implants was assessed 8 d later by ultrasonography and further confirmed by histologic examination (Fig. 7F). Compared with the PBS group, which exhibited vascularization of the Matrigel implants, a significantly lower degree of vascularity was observed in the N-LMP1 group (Fig. 7F, 7G). Altogether, these results suggest that N-LMP1–specific CD4 T cells may target angiogenic stroma independently of direct attack against tumor cells.

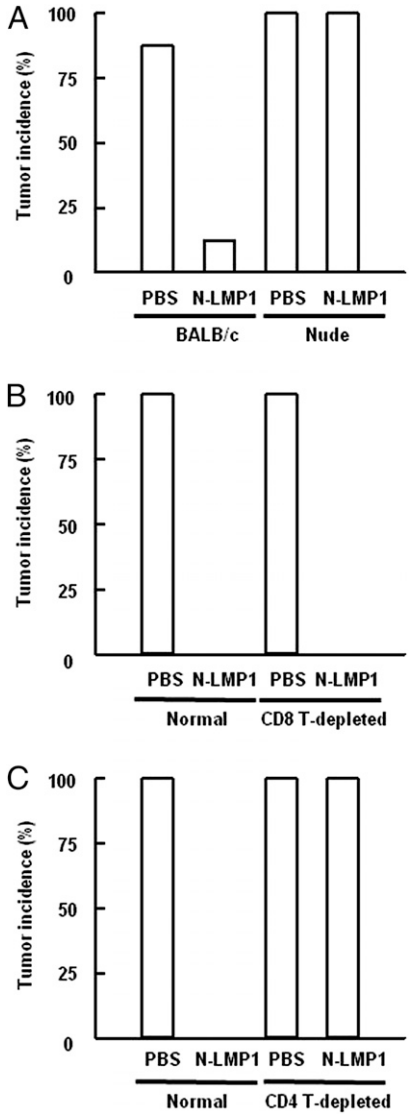

FIGURE 4. The T cell subset activated by N-LMP1. (**A**) BALB/c or nude mice ($n = 9$) were immunized with PBS or N-LMP1 TSCs (N-LMP1) before tumor challenge. BALB/c mice ($n = 4$) were depleted of CD8 (**B**) or CD4 T cells (**C**) by Ab treatment prior to immunization and tumor challenge. The tumor incidence was recorded on day 30 post transplantation.

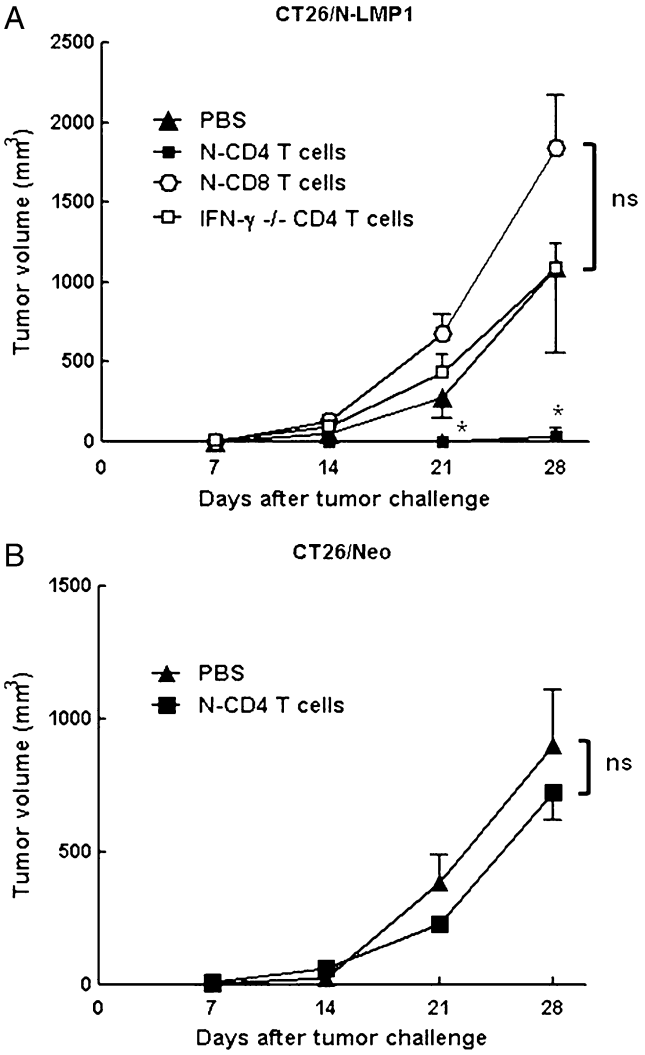

FIGURE 5. The immunogenicity of N-LMP1 and CD4 T cell immune surveillance. (**A**) SCID mice were i.v. injected with normal CD4 T cells, normal CD8 T cells, IFN-γ–deficient CD4 T cells (20×10^6/mouse), or PBS 1 h before CT26/N-LMP1 tumor induction. (**B**) SCID mice were challenged with CT26/Neo after adoptive transfer of normal CD4 T cells ($n = 4$). Statistically significant differences between each group and the PBS control are indicated. $^*p < 0.05$.

Discussion

The oncogenicity of N-LMP1 is crucial for NPC development in Taiwan (11). The aim of this study was to explore the effect of its in vivo immunogenicity on the course of N-LMP1–directed tumor progression. We used a tumor model that was established by in vivo tumorigenesis of N-LMP1–transformed BALB/c-3T3 cells in syngeneic immunocompetent hosts (18), highlighting the interaction between N-LMP1 and the immune system during tumor progression. Using an immunization approach, we demonstrated for the first time, to our knowledge, N-LMP1–mediated induction of an antiangiogenic response in CD4 T cells, providing important insights into the in vivo role of anti-LMP1 T cell immunity in EBV-associated malignancies.

Our data suggest that N-LMP1 may bear immunogenicity in addition to oncogenicity (15). This finding is consistent with a previous clinical study that LMP1-positive tumors exhibit a faster expansion pattern, but a lower frequency of recurrence and metastasis, compared with LMP1-negative tumors (35). However, using an experimental mouse model, several reports have described the nonimmunogenicity or low immunogenicity of NPC-derived LMP1 variants (13, 14). This discrepancy may be a result of the different LMP1 sequences and the genetic backgrounds in the cell lines and mouse strains used in the studies. Nevertheless, despite the fast and profound antitumor immunity elicited by N-LMP1, the response does not seem to be sustained following immunization (Fig. 3B). The decline of the tumor-free rate with time suggests that the immunosuppressive properties demonstrated by other NPC-derived LMP1 variants (13, 14, 36, 37) may still be preserved in N-LMP1. However, the regulatory T cell response is eventually induced (38), creating an immunogenic window in the early exposure of N-LMP1 to the immune system.

CD8 T cells have been considered the main effectors that protect against LMP1-associated malignancies (9), with little attention paid to relating CD4 responses. Our major finding is that the N-LMP1–specific CD4 T cells have an effector role in monitoring tumor neovascularization. Intriguingly, the current study (Fig. 5), as well as others (29, 33, 39, 40), showed that normal CD4 T cells are involved in tumor prevention. This finding agrees with our previous observation that a naive host could reject a tumor in-

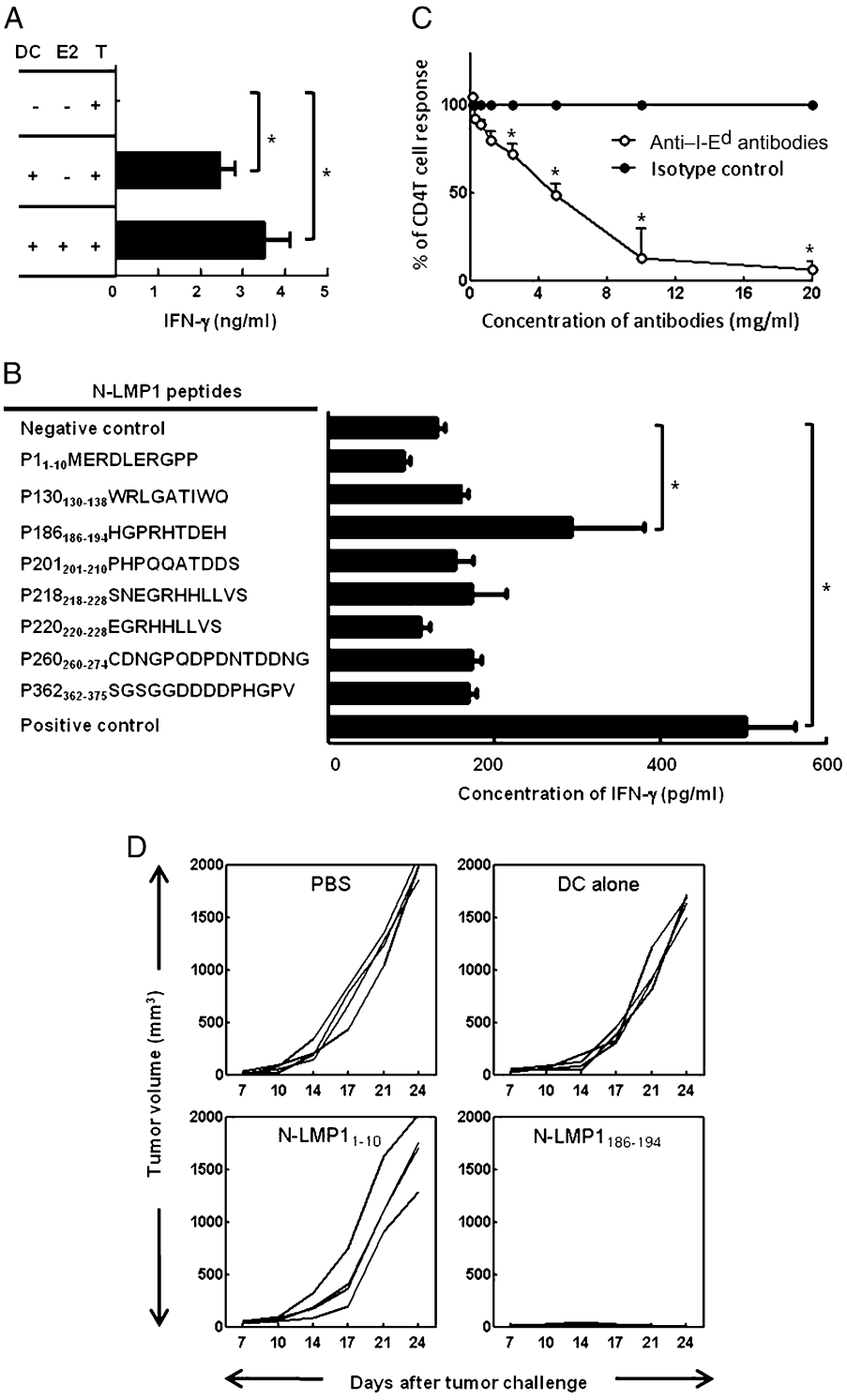

FIGURE 6. Identification of the N-LMP1 peptide responsible for the CD4 T cell response. CD4 T cells from N-LMP1–immunized BALB/c mice were in vitro stimulated with DCs that were (**A**) pre-incubated with or without E2-plus lysate or (**B**) pulsed with various synthetic peptides derived from N-LMP1. The supernatants were harvested on day 3, and IFN-γ production was determined by ELISA. In (B), the negative and positive controls were CD4 T cells with plain DCs or E2-plus–pulsed DCs, respectively. Statistically significant differences between each group and the negative control are indicated. (**C**) Serial dilutions of an anti–I-E^d blocking or isotype control Ab were added to cultures of CD4 T cells with N-LMP1$_{186–194}$–pulsed DCs. The percent of CD4 T cell response was calculated using isotype controls as 100%. The results are the mean ±SD of triplicate determinations of three independent experiments. (**D**) BALB/c mice were immunized with PBS, with DCs alone, or with N-LMP1$_{1–10}$- or N-LMP1$_{186–194}$–pulsed DCs, and challenged with tumors 4 d later. In (D), tumor growth curves ($n = 4$) are presented as a function of time. *$p < 0.05$.

duced by monosuspended tumor cells (18). However, this defense may target early events, becoming insufficient against more advanced stages, owing to the high rate of tumor incidence displayed in mice receiving tumor fragment transplantation (18). It appears that tumor fragment provides stroma that favors tumor development (41). Nevertheless, we showed that the protumor condition could be neutralized (42) via immunization that generates IFN-γ–producing CD4 T effectors blocking angiogenesis. As N-LMP1 tumor does not express MHC-II even with IFN-γ stimulation (Fig. 7), it is unlikely that the diminishing angiogenesis is caused by direct recognition and killing of tumor cells by CD4 T cells (39, 40). Tumor-infiltrating macrophages have been shown to play an Ag-presenting role in an MHC-II–negative tumor model (39). In our model system, the major infiltrating cells are CD11b-positive myeloid cells (18). It has been demonstrated that the recruitment of these cells into the tumor microenvironment is crucial for de novo vessel formation and angiogenic switch (43). Consistent with this idea, we also observed early stepwise deposits of myeloid cells close to the vessel lumen (44), and the timeline of deposition matches the timeline of the multiple high K^{trans} peaks developing from day 7 to day 14 (Fig. 1). In this study, we further demonstrated that the majority of $CD11b^+$ stromal cells express

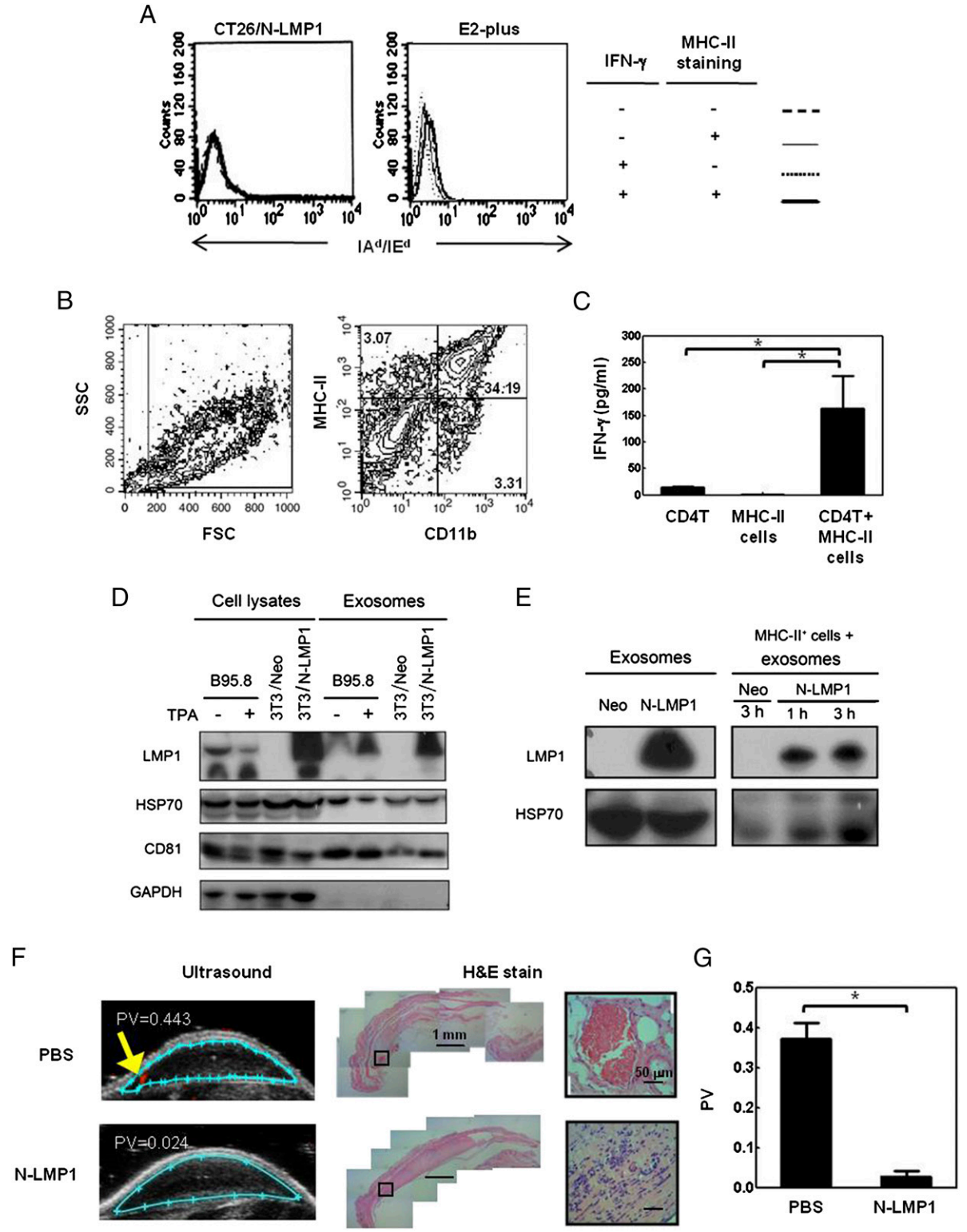

FIGURE 7. The target of N-LMP1–specific CD4 T cells. (**A**) CT26/N-LMP1 or E2-plus cells were cultured with or without IFN-γ (200 U/ml). At 2 d later, cells were collected for MHC-II staining. (**B**) TSCs were double stained for MHC-II and CD11b. (**C**) DC/peptide-primed CD4 T cells were cultured with or without sorted MHC-II$^+$ cells. The supernatants were harvested on day 3 and tested for IFN-γ by ELISA. Data are expressed as the mean ±SD of triplicate determinations of three independent experiments. (**D**) Cell lysates and purified exosomes from conditioned media of 3T3/Neo or 3T3/N-LMP1 were analyzed by immunoblotting for LMP1 and exosome markers (HSP70 and CD81). B95.8 cells, with or without TPA treatment, were used as positive controls for the detection of LMP1. The ratio of full-length LMP1 (*upper band*) versus lytic form of LMP1 (*lower band*) is decreased by treatment with TPA (22). GAPDH was used as the loading control of immunoblot. (**E**) MHC-II$^+$ cells were treated with purified exosomes from 3T3/Neo (Neo) or 3T3/N-LMP1 (N-LMP1) for 1 h and 3 h. Cells were stringently washed, and total proteins were harvested for immunoblot analysis. HSP70 was used as the loading control for Western blotting. (**F**) BALB/c mice (n = 3) were immunized with PBS or N-LMP1 TSCs (N-LMP1). At 4 d later, mice were injected (s.c.) with MHC-II$^+$ cell–embedded Matrigel as described in *Materials and Methods*. At 8 d after implantation, the blood vessels (arrow) developed within the Matrigel (defined by blue lines) were visualized by ultrasonography. H&E-stained Matrigel sections and higher magnification of the *inset* (original magnification ×20) are shown. (**G**) The vascularity was quantified using the PV value (the volume ratio of blood-flowing vessels (*Figure legend continues*)

MHC-II. Moreover, they can uptake LMP1 released by tumor cells via exosomes, which may have facilitated the acquisition of the LMP1 Ag by stromal cells for CD4 T cell recognition. Although N-LMP1 could not be detected in MHC-II$^+$ cells (as shown in the control group with 3T3/Neo exosomes, Fig. 7E), their ability to present the N-LMP1 Ag is revealed by the stimulation of IFN-γ production in N-LMP1$_{186–194}$–loaded DC-primed CD4 T cells (Fig. 7C). Immunization with N-LMP1$_{186–194}$–pulsed DCs successfully inhibited tumor progression (Fig. 6D), further supporting the natural processing and presentation of N-LMP1 protein by tumor tissues to CD4 T cells. More importantly, we showed that the MHC-II$^+$ cells can stimulate vascularization. By contrast, the activity is dampened in the immune host, confirming that N-LMP1–specific CD4 T cells target MHC-II$^+$ stromal cells in the angiogenic control. Our results support the importance of IFN-γ in CD4 T-mediated angiogenic blockade. IFN-γ may impair tumor neovascularization by alteration of endothelial cell function (45), modulation of proinflammatory microenvironment (31, 46), and/or disruption of the angiogenic process involving stromal cells that bear IFNRs (32).

The more prominent role of CD4 than CD8 T cells may be inferred from the prior activation of CD4 T, which is in general required for CD8 T activation. It is likely that the control of early tumor angiogenesis demands early T cell infiltration (30, 31). Nevertheless, CD4 T cell response may lead only to tumor dormancy (31). The successive infiltration of CD8 T cells may be necessary to sustain long-term immune protection (33, 47), providing an explanation for the slightly less powerful tumor inhibition on day 28 in the SCID mice receiving only CD4 T cell transfer (Fig. 5). Recently, some proangiogenic myeloid stromal cells have been shown to uptake and cross-present tumor Ags via the MHC-I molecule, leading to an antitumor CD8 T cell response, including the prevention of neovascularization through cell elimination (33). It is worth noting that the stromal cells identified by the MHC-I–restricted TCR tetramer are also MHC-II positive (48), implying the possibility of recognizing common stromal cells in the collaboration of CD4 and CD8T cells during the process of angiogenic surveillance.

Our results demonstrate that N-LMP1 bears immunogenicity, inducing an IFN-γ–mediated CD4 T cell surveillance against tumor angiogenesis. This potential clinical benefit provides a rationale for the use of LMP1-based immunotherapy for cancer treatment (6, 49, 50). This study also demonstrates the antigenic and angiogenic activity of the MHC-II$^+$ stromal cells, thus supporting therapies such as the emerging T cell therapy that targets tumor stroma (33, 51).

Acknowledgments

We thank Kuan-Yin Shen, Chia-Ming Shih, Mei-Lun Tseng, and Chia-Yin Lee for technical assistance.

Disclosures

The authors have no financial conflicts of interest.

References

1. Dawson, C. W., R. J. Port, and L. S. Young. 2012. The role of the EBV-encoded latent membrane proteins LMP1 and LMP2 in the pathogenesis of nasopharyngeal carcinoma (NPC). *Semin. Cancer Biol.* 22: 144–153.
2. Li, H. P., and Y. S. Chang. 2003. Epstein-Barr virus latent membrane protein 1: structure and functions. *J. Biomed. Sci.* 10: 490–504.
3. Liu, S. C., N. M. Tsang, W. C. Chiang, K. P. Chang, C. Hsueh, Y. Liang, J. L. Juang, K. P. Chow, and Y. S. Chang. 2013. Leukemia inhibitory factor promotes nasopharyngeal carcinoma progression and radioresistance. *J. Clin. Invest.* 123: 5269–5283.
4. Hannigan, A., A. M. Qureshi, C. Nixon, P. M. Tsimbouri, S. Jones, A. W. Philbey, and J. B. Wilson. 2011. Lymphocyte deficiency limits Epstein-Barr virus latent membrane protein 1 induced chronic inflammation and carcinogenic pathology in vivo. *Mol. Cancer* 10: 11.
5. Pai, S., B. J. O'Sullivan, L. Cooper, R. Thomas, and R. Khanna. 2002. RelB nuclear translocation mediated by C-terminal activator regions of Epstein-Barr virus-encoded latent membrane protein 1 and its effect on antigen-presenting function in B cells. *J. Virol.* 76: 1914–1921.
6. Long, H. M., G. S. Taylor, and A. B. Rickinson. 2011. Immune defence against EBV and EBV-associated disease. *Curr. Opin. Immunol.* 23: 258–264.
7. Duraiswamy, J., J. M. Burrows, M. Bharadwaj, S. R. Burrows, L. Cooper, N. Pimtanothai, and R. Khanna. 2003. Ex vivo analysis of T-cell responses to Epstein-Barr virus-encoded oncogene latent membrane protein 1 reveals highly conserved epitope sequences in virus isolates from diverse geographic regions. *J. Virol.* 77: 7401–7410.
8. Haigh, T. A., X. Lin, H. Jia, E. P. Hui, A. T. Chan, A. B. Rickinson, and G. S. Taylor. 2008. EBV latent membrane proteins (LMPs) 1 and 2 as immunotherapeutic targets: LMP-specific CD4+ cytotoxic T cell recognition of EBV-transformed B cell lines. *J. Immunol.* 180: 1643–1654.
9. Hislop, A. D., G. S. Taylor, D. Sauce, and A. B. Rickinson. 2007. Cellular responses to viral infection in humans: lessons from Epstein-Barr virus. *Annu. Rev. Immunol.* 25: 587–617.
10. Lin, X., N. H. Gudgeon, E. P. Hui, H. Jia, X. Qun, G. S. Taylor, M. C. Barnardo, C. K. Lin, A. B. Rickinson, and A. T. Chan. 2008. CD4 and CD8 T cell responses to tumour-associated Epstein-Barr virus antigens in nasopharyngeal carcinoma patients. *Cancer Immunol. Immunother.* 57: 963–975.
11. Chen, M. L., C. N. Tsai, C. L. Liang, C. H. Shu, C. R. Huang, D. Sulitzeanu, S. T. Liu, and Y. S. Chang. 1992. Cloning and characterization of the latent membrane protein (LMP) of a specific Epstein-Barr virus variant derived from the nasopharyngeal carcinoma in the Taiwanese population. *Oncogene* 7: 2131–2140.
12. Miller, W. E., R. H. Edwards, D. M. Walling, and N. Raab-Traub. 1994. Sequence variation in the Epstein-Barr virus latent membrane protein 1. *J. Gen. Virol.* 75: 2729–2740.
13. Trivedi, P., L. F. Hu, F. Chen, B. Christensson, M. G. Masucci, G. Klein, and G. Winberg. 1994. Epstein-Barr virus (EBV)-encoded membrane protein LMP1 from a nasopharyngeal carcinoma is non-immunogenic in a murine model system, in contrast to a B cell-derived homologue. *Eur. J. Cancer* 30A: 84–88.
14. Hu, L., B. Troyanovsky, X. Zhang, P. Trivedi, I. Ernberg, and G. Klein. 2000. Differences in the immunogenicity of latent membrane protein 1 (LMP1) encoded by Epstein-Barr virus genomes derived from LMP1-positive and -negative nasopharyngeal carcinoma. *Cancer Res.* 60: 5589–5593.
15. Li, S. N., Y. S. Chang, and S. T. Liu. 1996. Effect of a 10-amino acid deletion on the oncogenic activity of latent membrane protein 1 of Epstein-Barr virus. *Oncogene* 12: 2129–2135.
16. Chen, C. C., H. P. Liu, M. Chao, Y. Liang, N. M. Tsang, H. Y. Huang, C. C. Wu, and Y. S. Chang. 2014. NF-κB-mediated transcriptional upregulation of TNFAIP2 by the Epstein-Barr virus oncoprotein, LMP1, promotes cell motility in nasopharyngeal carcinoma. *Oncogene* 33: 3648–3659.
17. Folkman, J., K. Watson, D. Ingber, and D. Hanahan. 1989. Induction of angiogenesis during the transition from hyperplasia to neoplasia. *Nature* 339: 58–61.
18. Chow, K. P., C. C. Wu, H. Y. Chang, C. Chang, and Y. S. Chang. 2008. A simplified tumour model established via Epstein-Barr virus-encoded, nasopharyngeal carcinoma-derived oncogene latent membrane protein 1 in immunocompetent mice. *Lab. Anim.* 42: 193–203.
19. Sathy, B. N., Y. H. Chou, H. J. Li, C. Chang, and K. P. Chow. 2009. Dynamic contrast-enhanced and T2-weighted magnetic resonance imaging study of the correlation between tumour angiogenesis and growth kinetics. *Lab. Anim.* 43: 53–59.
20. Lin, W. C., T. P. Pretlow, T. G. Pretlow, II, and L. A. Culp. 1990. Bacterial lacZ gene as a highly sensitive marker to detect micrometastasis formation during tumor progression. *Cancer Res.* 50: 2808–2817.
21. Hsieh, Y. H., C. J. Wu, K. P. Chow, C. L. Tsai, and Y. S. Chang. 2003. Electroporation-mediated and EBV LMP1-regulated gene therapy in a syngenic mouse tumor model. *Cancer Gene Ther.* 10: 626–636.
22. Vazirabadi, G., T. R. Geiger, W. F. Coffin, III, and J. M. Martin. 2003. Epstein-Barr virus latent membrane protein-1 (LMP-1) and lytic LMP-1 localization in plasma membrane-derived extracellular vesicles and intracellular virions. *J. Gen. Virol.* 84: 1997–2008.
23. Meckes, D. G., Jr., K. H. Shair, A. R. Marquitz, C. P. Kung, R. H. Edwards, and N. Raab-Traub. 2010. Human tumor virus utilizes exosomes for intercellular communication. *Proc. Natl. Acad. Sci. USA* 107: 20370–20375.
24. Tofts, P. S., and A. G. Kermode. 1991. Measurement of the blood-brain barrier permeability and leakage space using dynamic MR imaging. 1. Fundamental concepts. *Magn. Reson. Med.* 17: 357–367.
25. Bernick, S. 1966. Vascular and nerve supply to the molar teeth of guinea pigs. *J. Dent. Res.* 45: 249–260.

versus the whole Matrigel implant). Data in (A), (B), and (F) are representative of three independent experiments. Immunoblots are representative of two independent experiments. Statistically significant difference between the N-LMP1 group and PBS control is indicated ($n = 3$). *$p < 0.05$.

26. Chow, K. P., J. M. Lee, J. T. Qiu, S. K. Liao, S. C. Lin, S. L. Hsu, N. N. Wu, Y. F. Lin, and T. S. Wu. 2011. Enhanced IL-10 production by CD4+ T cells primed in IL-15Rα-deficient mice. *Eur. J. Immunol.* 41: 3146–3156.
27. Xiao, D., J. Ohlendorf, Y. Chen, D. D. Taylor, S. N. Rai, S. Waigel, W. Zacharias, H. Hao, and K. M. McMasters. 2012. Identifying mRNA, microRNA and protein profiles of melanoma exosomes. *PLoS ONE* 7: e46874.
28. Yin, Y., X. Huang, K. D. Lynn, and P. E. Thorpe. 2013. Phosphatidylserine-targeting antibody induces M1 macrophage polarization and promotes myeloid-derived suppressor cell differentiation. *Cancer Immunol Res* 1: 256–268.
29. Shankaran, V., H. Ikeda, A. T. Bruce, J. M. White, P. E. Swanson, L. J. Old, and R. D. Schreiber. 2001. IFNgamma and lymphocytes prevent primary tumour development and shape tumour immunogenicity. *Nature* 410: 1107–1111.
30. Beatty, G., and Y. Paterson. 2001. IFN-gamma-dependent inhibition of tumor angiogenesis by tumor-infiltrating CD4+ T cells requires tumor responsiveness to IFN-gamma. *J. Immunol.* 166: 2276–2282.
31. Müller-Hermelink, N., H. Braumüller, B. Pichler, T. Wieder, R. Mailhammer, K. Schaak, K. Ghoreschi, A. Yazdi, R. Haubner, C. A. Sander, et al. 2008. TNFR1 signaling and IFN-gamma signaling determine whether T cells induce tumor dormancy or promote multistage carcinogenesis. *Cancer Cell* 13: 507–518.
32. Qin, Z., and T. Blankenstein. 2000. CD4+ T cell–mediated tumor rejection involves inhibition of angiogenesis that is dependent on IFN gamma receptor expression by nonhematopoietic cells. *Immunity* 12: 677–686.
33. Zhang, B., Y. Zhang, N. A. Bowerman, A. Schietinger, Y. X. Fu, D. M. Kranz, D. A. Rowley, and H. Schreiber. 2008. Equilibrium between host and cancer caused by effector T cells killing tumor stroma. *Cancer Res.* 68: 1563–1571.
34. Yoshizaki, T., S. Kondo, N. Wakisaka, S. Murono, K. Endo, H. Sugimoto, S. Nakanishi, A. Tsuji, and M. Ito. 2013. Pathogenic role of Epstein-Barr virus latent membrane protein-1 in the development of nasopharyngeal carcinoma. *Cancer Lett.* 337: 1–7.
35. Hu, L. F., F. Chen, Q. F. Zhen, Y. W. Zhang, Y. Luo, X. Zheng, G. Winberg, I. Ernberg, and G. Klein. 1995. Differences in the growth pattern and clinical course of EBV-LMP1 expressing and non-expressing nasopharyngeal carcinomas. *Eur. J. Cancer* 31A: 658–660.
36. Pai, S., B. O'Sullivan, I. Abdul-Jabbar, J. Peng, G. Connoly, R. Khanna, and R. Thomas. 2007. Nasopharyngeal carcinoma-associated Epstein-Barr virus-encoded oncogene latent membrane protein 1 potentiates regulatory T-cell function. *Immunol. Cell Biol.* 85: 370–377.
37. Middeldorp, J. M., and D. M. Pegtel. 2008. Multiple roles of LMP1 in Epstein-Barr virus induced immune escape. *Semin. Cancer Biol.* 18: 388–396.
38. Casares, N., L. Arribillaga, P. Sarobe, J. Dotor, A. Lopez-Diaz de Cerio, I. Melero, J. Prieto, F. Borrás-Cuesta, and J. J. Lasarte. 2003. CD4+/CD25+ regulatory cells inhibit activation of tumor-primed CD4+ T cells with IFN-gamma-dependent antiangiogenic activity, as well as long-lasting tumor immunity elicited by peptide vaccination. *J. Immunol.* 171: 5931–5939.
39. Corthay, A., D. K. Skovseth, K. U. Lundin, E. Røsjø, H. Omholt, P. O. Hofgaard, G. Haraldsen, and B. Bogen. 2005. Primary antitumor immune response mediated by CD4+ T cells. *Immunity* 22: 371–383.
40. Xie, Y., A. Akpinarli, C. Maris, E. L. Hipkiss, M. Lane, E. K. Kwon, P. Muranski, N. P. Restifo, and P. A. Antony. 2010. Naive tumor-specific CD4(+) T cells differentiated in vivo eradicate established melanoma. *J. Exp. Med.* 207: 651–667.
41. Singh, S., S. R. Ross, M. Acena, D. A. Rowley, and H. Schreiber. 1992. Stroma is critical for preventing or permitting immunological destruction of antigenic cancer cells. *J. Exp. Med.* 175: 139–146.
42. Coussens, L. M., L. Zitvogel, and A. K. Palucka. 2013. Neutralizing tumor-promoting chronic inflammation: a magic bullet? *Science* 339: 286–291.
43. Melero-Martin, J. M., and A. C. Dudley. 2011. Concise review: vascular stem cells and tumor angiogenesis. *Stem Cells* 29: 163–168.
44. Shih, Y. Y., Y. H. Hsu, T. Q. Duong, S. S. Lin, K. P. Chow, and C. Chang. 2011. Longitudinal study of tumor-associated macrophages during tumor expansion using MRI. *NMR Biomed.* 24: 1353–1360.
45. Rüegg, C., A. Yilmaz, G. Bieler, J. Bamat, P. Chaubert, and F. J. Lejeune. 1998. Evidence for the involvement of endothelial cell integrin alphaVbeta3 in the disruption of the tumor vasculature induced by TNF and IFN-gamma. *Nat. Med.* 4: 408–414.
46. Enzler, T., S. Gillessen, J. P. Manis, D. Ferguson, J. Fleming, F. W. Alt, M. Mihm, and G. Dranoff. 2003. Deficiencies of GM-CSF and interferon gamma link inflammation and cancer. *J. Exp. Med.* 197: 1213–1219.
47. Barth, R. J., Jr., J. J. Mulé, P. J. Spiess, and S. A. Rosenberg. 1991. Interferon gamma and tumor necrosis factor have a role in tumor regressions mediated by murine CD8+ tumor-infiltrating lymphocytes. *J. Exp. Med.* 173: 647–658.
48. Zhang, B., N. A. Bowerman, J. K. Salama, H. Schmidt, M. T. Spiotto, A. Schietinger, P. Yu, Y. X. Fu, R. R. Weichselbaum, D. A. Rowley, et al. 2007. Induced sensitization of tumor stroma leads to eradication of established cancer by T cells. *J. Exp. Med.* 204: 49–55.
49. Smith, C., J. Tsang, L. Beagley, D. Chua, V. Lee, V. Li, D. J. Moss, W. Coman, K. H. Chan, J. Nicholls, et al 2012. Effective treatment of metastatic forms of Epstein-Barr virus-associated nasopharyngeal carcinoma with a novel adenovirus-based adoptive immunotherapy. *Cancer Res.* 72: 1116–1125.
50. Tsang, J., V. H. Lee, and D. L. Kwong. 2014. Novel therapy for nasopharyngeal carcinoma—where are we. *Oral Oncol.* 50: 798–801.
51. Engels, B., D. A. Rowley, and H. Schreiber. 2012. Targeting stroma to treat cancers. *Semin. Cancer Biol.* 22: 41–49.